Modeling and optimization of electro-optic phase modulator

P. Shames, P.C. Sun, and Y. Fainman

University of California, San Diego, Electrical and Computer Engineering Dept.
9500 Gilman Dr., La Jolla, California 92093

ABSTRACT

We introduce a novel method of modeling PLZT phase modulators. Traditionally, modeling has been based upon fitting the constant quadratic electro-optic coefficient to empirical data. Our characterization has shown that the electro-optic coefficient is not a constant and that the electro-optic effect saturates at electric field strengths that exist in standard surface electrode device configurations. We have also found that the additional effects of light scattering and depolarization, which depend on the strength of the applied electric field, are significant factors for modeling device design and optimization.

Keywords: PLZT, electro-optic effect, phase modulators, finite element analysis, depolarization, scattering.

1. INTRODUCTION

PLZT is an excellent material choice for use in spatial light modulators (SLM) due to it's large electro-optic effect and low absorption for thin wafers[1]. PLZT ceramics are used as transverse electro-optic modulators where the electric field is applied using interdigital surface electrodes (ISE). Such electro-optic devices are modeled based upon the quadratic electro-optic effect[2-6] as well as it's combination with the linear electro-optic effect[7]. However these models do not accurately predict the performance of an ISE device fabricated at UCSD[8]. In order to more accurately model such devices we experimentally characterized PLZT's electro-optic properties. Then we used finite element analysis (FEA) to characterize the field distributions for ISE devices. Finally, by combining the electric field values provided by FEA with the experimental electro-optic data, we were able to predict the performance of our ISE device. Although this methodology was carried out with PLZT 9.0/65/35 material, it can be applied to modeling electro-optic devices with arbitrary choice of material, electrode structure and geometry.

In the following section we will review the basic theory of quadratic electro-optic materials, as well as formulate the methodology for characterization of PLZT electro-optic material. In section 3, we will apply FEA to model the electric field induced by an electric potential difference between electrodes of ISE devices. The results of section 2 are integrated into the FEA model to determine the relationship between the change in relative phase of two orthogonally polarized components of an incident beam and the externally applied electric field. In section 4 we compare this prediction with the actual values taken from the fabricated ISE device. Conclusions and future directions are discussed in section 5.

2. CHARACTERIZATION OF ELECTRO-OPTIC MATERIAL

G. Haertling and C. Land initiated extensive studies characterizing PLZT ceramics[1]. They found that thin wafers with compositions containing greater than 8 at.% La had strong electro-optic properties with transmission values of close to 100%. At room temperature, PLZT is isotropic due to it's cubic crystallographic structure. When an external electric field is applied the PLZT material becomes polarized, demonstrating anisotropic optical characteristics. This same behavior is seen in crystals such as $BaTiO_3$ (in it's cubic form) that exhibit primarily third order non-linear optical properties which in turn lead to quadratic electro-optic effects. Assuming PLZT follows this uniaxial crystal model, the optic axis will be determined by the direction of an externally applied electric field. The induced ordinary and extraordinary index of refraction is determined by

$$n_o = n - \tfrac{1}{2} n^3 R_{12} E^2 \quad \text{and} \quad n_e = n - \tfrac{1}{2} n^3 R_{11} E^2 \qquad (1)$$

$$\Delta n(E) = n_o - n_e = \tfrac{1}{2} n^3 R E^2 \qquad (2)$$

where $R \equiv R_{12} - R_{11}$, R_{12} and R_{11} are the quadratic electro-optic coefficients, n is the refractive index of PLZT, and $\Delta n(E)$ is the induced optical birefringence. For PLZT with 9.0 at.% La the accepted value[13] for R is approximately 3.8×10^{16} m^2/V^2. Haertling and Land[1] noticed that the induced optical birefringence saturates with an externally applied electric field reaching a maximum[7] value of 1.1×10^{-2} . More recently, M. Title[5] mentioned the saturation effect in modeling embedded electrode PLZT modulators.

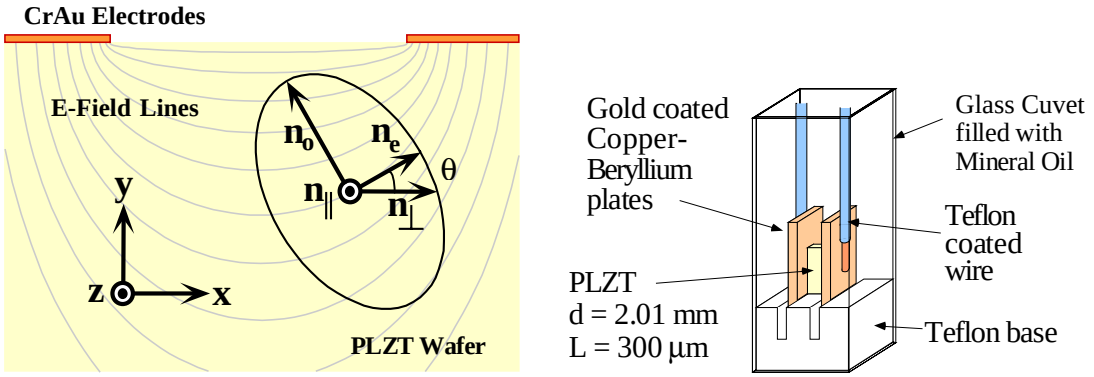

Figure 1. (a) For ISE on PLZT the index ellipsoid follows the tangent of the curved E-field lines. (b) PLZT wafer, 300 μm thick and 2.01 mm wide, placed between gold coated copper plates. The plates were inserted into a Teflon base to ensure good electrical isolation and the cuvet was filled with mineral oil to prevent current arcing due to exceeding the breakdown voltage of air.

A typical ISE device is constructed of stripe-shaped metal electrodes of width d and length L. An applied voltage across such electrodes creates curved lines of electric field within the PLZT (see Figure 1a). Since the optic axis follows the direction of the applied electric field, the axis orientation will vary as a function of position within the PLZT. Assuming the electrode length

$L >> d$, the index of refraction parallel and perpendicular to the surface electrodes can be approximated[5] by

$$n_{\parallel} = n_o \quad \text{and} \quad n_{\perp} = \left[\frac{\cos^2\left(\theta(x,y)\right)}{n_e^2} + \frac{\sin^2\left(\theta(x,y)\right)}{n_o^2} \right]^{-\frac{1}{2}} \qquad \textbf{(3)}$$

$$\text{where } \theta(x,y) = \text{Tan}^{-1}\left(\frac{E_y(x,y)}{E_x(x,y)} \right) \qquad \textbf{(4)}$$

Defining the relative change in index $\Delta n\left(\theta(x,y)\right) = n_{\perp} - n_{\parallel}$, we determine the relative phase between the parallel and perpendicular polarization components of an optical beam passing through the device by

$$\Phi(x) = \frac{2\pi}{\lambda} \int_{y=0}^{l} \Delta n\left(\theta(x,y)\right) dy \qquad \textbf{(5)}$$

where λ is the wavelength in vacuum and l is the thickness of the electrooptic material.

In the following we will experimentally determine the phase relationship provided by Equation 5. By placing the PLZT wafer between large parallel metal plates (see Figure 1b) a homogeneous electric field, perpendicular to the plates (i.e. $\theta = 0$), will exist within the dielectric. The field strength is a function of the potential difference between the plates (i.e. $E = \frac{V}{d}$, where d is the distance between the plates). To measure the induced phase retardation we illuminate the PLZT sample using a normally incident HeNe laser beam. The incident beam is linearly polarized at 45° with respect to the direction of the applied electric field, providing two equal components parallel and perpendicular with respect to the electrode structure. As the voltage, and thus the electric field strength, is varied, there will be a change in the relative phase between these two components.

By placing a crossed polarizer at the output of an ideal phase modulating device, the light intensity will vary as a function of the relative phase according[9] to the relation

$$T = \tfrac{1}{2}a^2 + \tfrac{1}{2}b^2 - ab\sin(\Phi) \qquad \textbf{(6)}$$

where Φ is the relative phase, and a^2 and b^2 are the transmittances for the two orthogonal components of the light. We measure the transmittance, T, through a crossed polarizer, as well as the transmittances through vertically and horizontally oriented polarizers, a^2 and b^2 respectively, as functions of the electric field. Then, by solving Equation 6 for Φ, we expect to find the relative phase as a function of electric field. However, using this method, the resultant phase is *not* continuous when a PLZT based device is being investigated. This is due to depolarization effects observed in PLZT phase modulators[10].

By introducing a depolarizing term into the transmittance of the orthogonal components in Equation 6, we obtain

$$T = \tfrac{1}{2}\left(a^2 + c_a^2\right) + \tfrac{1}{2}\left(b^2 + c_b^2\right) - ab\sin(\Phi) \quad \textbf{(7)}$$

where c_a and c_b are the fractions of depolarized light corresponding to the incident vertically and horizontally polarized components. Defining $A^2 = a^2 + c_a^2$ and $B^2 = b^2 + c_b^2$, we get the relationship

$$T = \tfrac{1}{2}A^2 + \tfrac{1}{2}B^2 - \sqrt{A^2 - c^2}\sqrt{B^2 - c^2}\sin(\Phi) \quad \textbf{(8)}$$

where we also assume that $c_a \approx c_b = c$. Using the measured values for T, A^2, B^2 and curve fit for c^2, we solve Equation 8 that provides continuous relative phase (see Figure 2b).

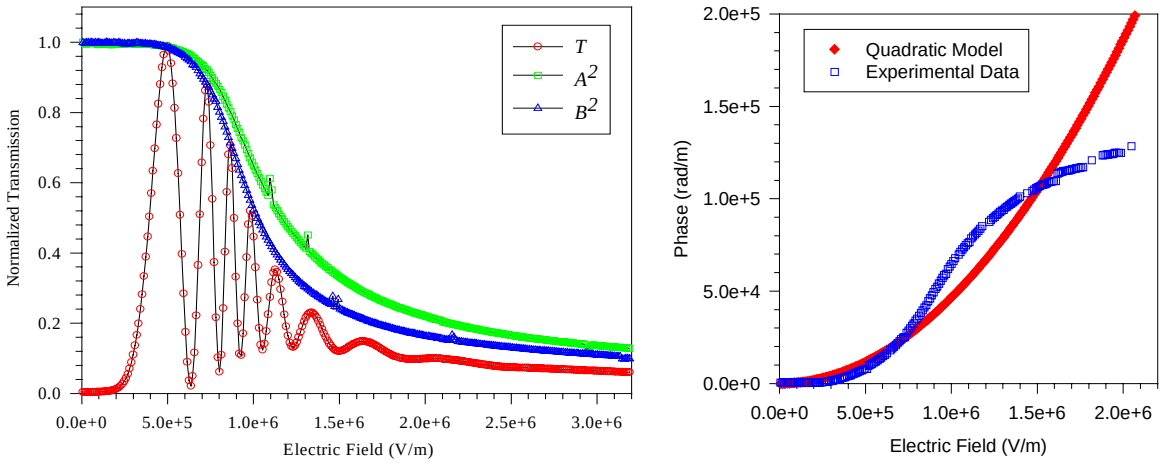

(a) (b)

Figure 2. (a) Transmittance T through crossed polarizers set at 45° and through parallel polarizers set vertically and horizontally, A^2 and B^2, as functions of a horizontally applied electric field. (b) Relative phase as a function of applied electric field. We also show the best fit for a quadratic electro-optic coefficient as $R = 6\times10^{-16}\ (\frac{\mathrm{V}}{\mathrm{m}})^2$.

Observing the two curves A^2 and B^2 of Figure 2a we notice a dramatic intensity drop after the electric field reaches approximately 7×10^5 V/m. The main reason for the attenuation is due to scattering effects. This also causes a corresponding drop in the transmittance, T, through the crossed polarizers. Furthermore, T varies sinusoidally with the period varying as a function of electric field. The frequency of the sine initially increases, whereas at fields above 1×10^6 V/m the frequency decreases. Above the value of 2×10^6 V/m the contrast ratio approaches 1:1, which is primarily due to the depolarization effects. Due to the need for high contrast ratios in phase modulators, scattering and depolarization effects must be factored into the design of such devices.

Figure 2b shows the relative phase vs. electric field, where the experimental data is determined by solving Equation 8. Below electric fields of 2×10^5 V/m there is practically no phase change in the PLZT. Above values of 1×10^6 V/m we observe that the phase change begins to saturate. Our calculations show that for PLZT surface electrode devices, there are regions where the field strengths are on the order of 2×10^6 V/m, and therefore, the saturation effect must also be taken into consideration in these devices.

3. FINITE ELEMENT ANALYSIS OF ELECTRO-OPTIC MODULATORS

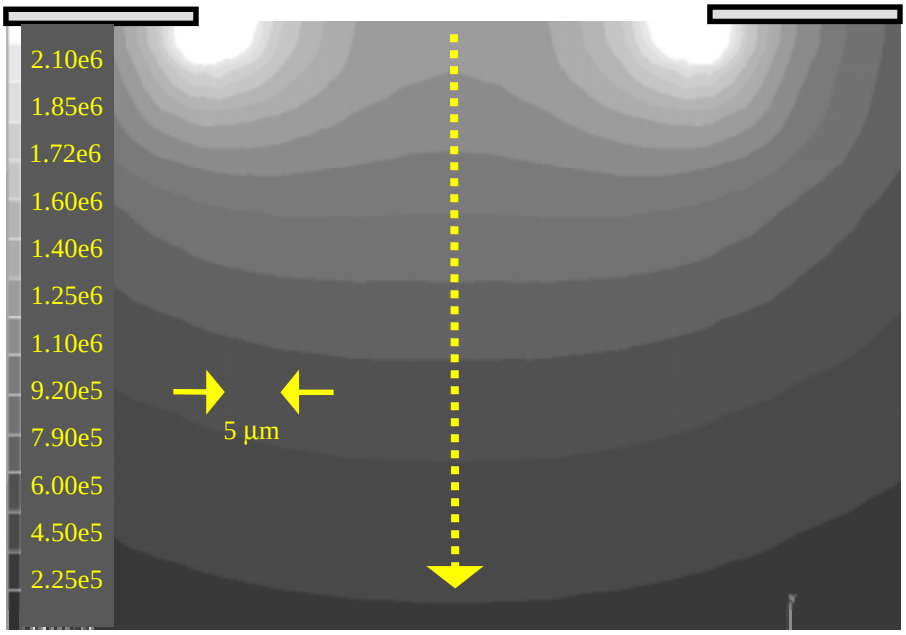

Figure 3. Mentat's output provides added insight into the effects of the electric field distribution. Shown is a portion of the contour band plot of the magnitude of the electric field between surface electrodes (outlined) 250 µm wide with a gap of 50 µm. For field strengths below 2.25×10^5 V/m there is no phase modulation and above 2.0×10^6 V/m the modulation has reached a maximum (see Figure 2b). Therefore, modulation only occurs within 100 µm of the surface and near the edges of the electrodes we observe electric field strengths beyond the 'saturation' level.

Finite Element Analysis (FEA) is one of several methods[3-6,11,12] available for calculating the electric field induced by metal electrodes. We use Mentat, a commercial FEA program from Marc Analysis, which provides an excellent tool for mesh generation, field calculations and visualization (see Figure 3). We used FEA to determine the electric field distribution in PLZT devices with surface electrodes. A typical example of Mentat's output is shown in Figure 3. For this particular ISE configuration, we observe that 100 µm from the surface the electric field strength drops below the minima required for phase modulation. We also see that near the edges of the electrodes the field goes beyond the maxima, i.e. the phase modulation has become constant. Using FEA we are able to calculate the electric field strength and direction, at any point, for any configuration of electrodes.

To find an explicit relationship between the magnitude and the direction of the electric field and the relative phase we substitute Eqs. 1, 2 and 3 into Equation 5 and obtain

$$\Phi(x)=\frac{2\pi}{\lambda}\int_{y=0}^{l}\left\{n_o\left[\cos^2\left(\theta(x,y)\right)\left(1-\frac{\Delta n(\theta=0)}{n_o}\right)^{-2}+\sin^2\left(\theta(x,y)\right)\right]^{-\frac{1}{2}}-n_o\right\}dy \qquad \textbf{(9)}$$

Using Taylor series expansion this can be approximated by

$$\begin{aligned}\Phi(x)&\approx\frac{2\pi}{\lambda}\int_{y=0}^{l}\left\{n_o\left[1+2\frac{\Delta n(\theta=0)}{n_o}\cos^2\left(\theta(x,y)\right)\right]^{-\frac{1}{2}}-n_o\right\}dy\\ &\approx\frac{2\pi}{\lambda}\int_{y=0}^{l}\Delta n(\theta=0)\cos^2\left(\theta(x,y)\right)dy=\frac{\pi}{\lambda}\int_{y=0}^{l}n^3R\left(E(x,y)\right)E^2(x,y)\cos^2\left(\theta(x,y)\right)dy\end{aligned} \qquad \textbf{(10)}$$

where we define the birefringence as quadratic, but with the electro-optic coefficient also being a function of the electric field. This can be more simply stated as

$$\Phi(x)=\int_{y=0}^{l}\phi\left(E(x,y)\right)\cos^2\left(\theta(x,y)\right)dy \qquad \textbf{(11)}$$

where $\phi\left(E(x,y)\right)$ is the phase function from the experimental curve of Figure 2b. Applying the electric field results from FEA we find

$$\Phi(x)\approx\sum_{i=1}^{N}\phi\left(E(x,y_i)\right)\cos^2\left(\theta(x,y_i)\right)l_i \qquad \textbf{(12)}$$

where N is the number of finite elements that the light ray passes through and l_i is the height of each element.

Mentat FEA software calculates the x and y components of the electric field (in this case we are using a two dimensional model) for four integration points for each element. Taking the average over each element we use the magnitude of the field (i.e. $E=\sqrt{E_x^2+E_y^2}$), the phase function and the orientation of the index ellipsoid from Equation 4 to get the relative phase change for each element. Integrating the change in phase passing through a column of elements, expressed by Equation 12, we find the change in phase for a light ray passing through a line of elements (see the dotted line in Figure 3). Looking at the series of columns across the electrode gap gives us a phase profile for a plane wave passing through the device.

4. MODELING VS. EXPERIMENTAL PERFORMANCES

Using the modeling procedures discussed in section 3 we determine the calculated phase distribution for a simulated ISE device and compare it to that found experimentally using a fabricated device. The FEA modeling and the experimentally measured results are found to be in good agreement for voltages of less than $V_{2\pi}$ and between electrode gaps of about 500 μm (see Figure 4a). For narrow gaps and higher voltages (see Figure 4b) there is a difference between the modeling and experimental results. One possible explanation would be that the electric field

strength is weaker then the value calculated by the FEA model due to screening effects. These screening effects occur when free carriers (photo-induced or due to surface states) create a space-charge distribution near the electrodes. Our future work will entail investigating these phenomena.

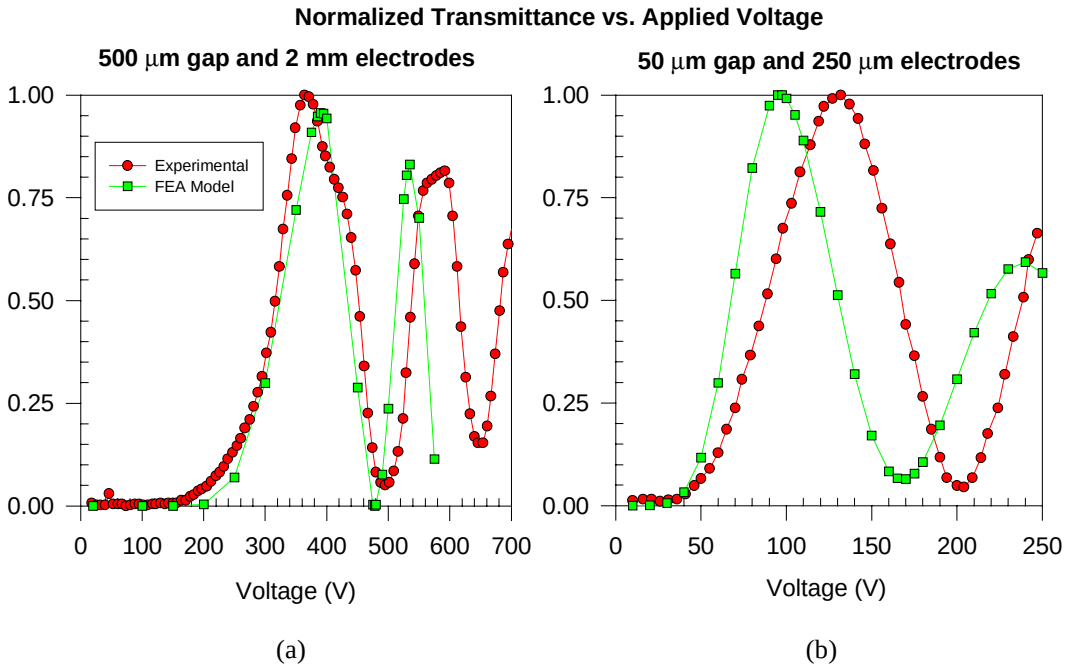

Figure 4. Comparison of FEA model to experimental data for transmission through crossed polarizers. (a) Shows a relatively good fit for V_{π} and $V_{2\pi}$ (i.e. the first maxima and minima) for an electrode gap of 500 μm. Whereas (b) shows a poor fit with a narrow electrode gap of 50 μm.

Currently, in our model, we are compensating for this 'weakening' effect by introducing a constant factor. Consequently, we are able to accurately model the behavior of fabricated devices operated at voltages less than $V_{2\pi}$ (see Figure 5a). Notice that the 'integrated phase' depends linearly on the applied voltage in contrast to the quadratic behavior predicted by previous models.

For surface electrode based devices, the two parameters that are most important are the electrode width and the size of the gap between electrodes. By varying the gap size, and holding the width (160 μm) and voltage (150 V) constant, in our FEA model we have determined that as the gap decreases the phase shift increases proportionately. This is expected based upon the linear relationship of phase to electric field, since the electric field strength scales proportionately with gap size. However, when the gap size becomes smaller than 40 μm there is very little increase in phase modulation. This is due to electric field values being above the 'saturation' level. We also find that as the electrodes increase in size there is a corresponding increase in phase shift, but electrodes wider than 160 μm were also of little benefit (see Figure 5b). The conclusion is that the optimal configuration for this material is a 40 μm gap between 160 μm

wide electrodes. It was experimentally determined[8] that for interdigital surface electrodes on PLZT 8.8/65/35 the optimum configuration is 160 μm electrode widths with 40 μm between electrode gaps. From this excellent agreement we conclude that optimization of design parameters can be done successfully using our FEA model.

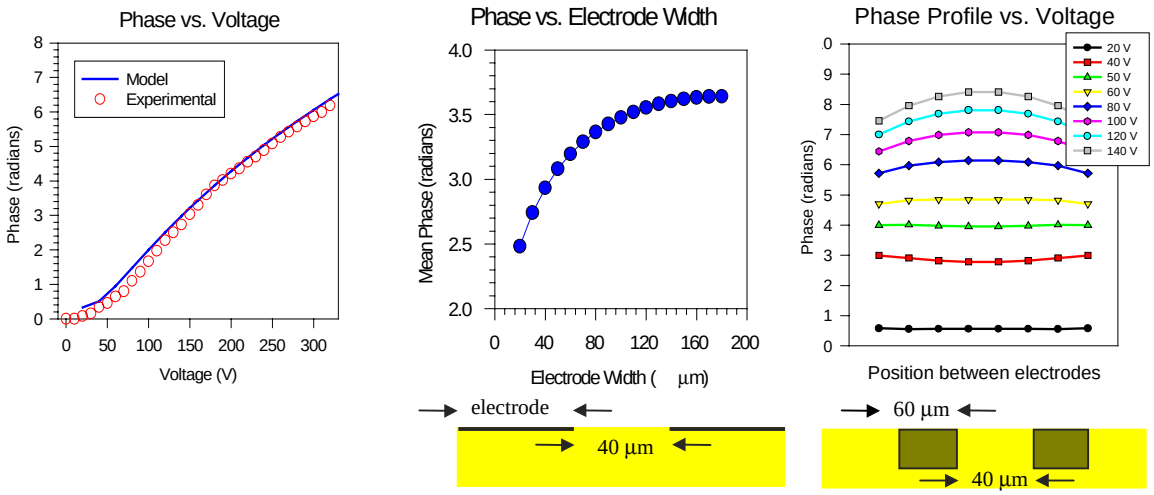

(a) (b) (c)

Figure 5. (a) Comparison of the FEA model with experimental data for phase as a function of applied voltage for surface electrodes 160 μm wide with a 40 μm gap (after including a compensating constant factor). (b) Holding the gap width (40 μm) and voltage (150 V) constant, the results of the FEA simulation show that as electrode width approaches 160 μm the increase in phase modulation slows down. (c) The gradient of the phase front for various applied voltages for etched electrodes 40 μm deep. A relatively flat phase profile across the entire gap can be realized around 50 Volts.

Gap Width (μm)	Electrode Width (μm)	Electrode Depth (μm)	V_π (V)
80	20	100	56.5
60	15	75	46.0
40	10	50	36.0
20	5	25	30.0

Table 1. The reduction in the necessary applied voltage to achieve π phase modulation highlights the advantages of 'scaling' down the electrode size and spacing.

With our general modeling approach, by varying other parameters within our FEA model we can design and evaluate many device configurations without having to fabricate many devices. In the following we will briefly discuss the optimization of two independent design criteria, embedded electrode geometry and phase uniformity. One of the limitations in using ISE devices is their low transmittance due to a small gap to electrode ratio, i.e. small fill factor. In contrast to surface electrodes, much larger fill factors can be realized by using electrodes that are embedded into the surface. To find the effect of using different etch depths we hold other parameters constant and change the scale of the electrode structure. Using a fill factor of 80% and assuming that a 5:1 aspect ratio is possible in etching PLZT substrate, we observe that V_π decreases steadily

as the gap gets smaller (see Table 1), indicating that the decrease in switching energy is proportional to the decrease in gap size. Under the constraint of an 80% fill factor we observe that the linear relationship no longer holds for a gap size below 40 μm. For small geometries the electric fields need to be high due to the short active modulation path length. Consequently, we once again observe the effects of 'saturation' of the phase modulation.

Another important characteristic of an electro-optic modulator is the homogeneity of the modulated phase front. Our FEA modeling allows us to calculate the phase distribution across the aperture between the electrodes. A plane wave passing through the gap between electrodes will attain a phase curvature across the aperture depending on the field distribution. According to our model, for a 50 μm wide gap at 150 Volts, there is a phase difference of approximately 0.7 radians from center to edge. By simulating various electrode geometries and applied voltages we find that by using electrodes 60 μm wide, spaced 40 μm apart and etched 40 μm deep the wave front has an almost perfectly flat π phase profile at 53.6 Volts (see Figure 5c). It is important to note here that we have been analyzing one characteristic at a time. In order to find an optimum device configuration, many coupled characteristics must be taken into account and weighted according to specific device requirements.

5. CONCLUSION

We have used a uniform applied electric field within PLZT in order to experimentally characterize the electro-optic response of the material. This characterization has highlighted the fact that scattering and depolarization effects need to be considered in determining the phase function. Furthermore, electric field distributions obtained using various electrode configurations have been calculated using FEA. These resultant electric fields were integrated with the phase function of the material to determine the characteristic phase modulation of an ISE electro-optic device. The calculated strength of the electric fields has shown us that 'saturation' of phase modulation needs to be considered in device design. We have also found that an electric field 'weakening' effect needs to be factored into the model and in the future we will investigate the cause of this phenomena. After compensating for these various effects we are able to model the behavior of a device as a function of a variety of parameters. We have shown that this model is useful in optimizing individually such device characteristics as increased transmittance and homogeneity of the phase front. Multiple characteristics of such devices that are mutually coupled can also be optimized.

8. ACKNOWLEDGMENTS

We wish to thank the invaluable help of Rebecca Bussjager at Rome Labs, Eddie Rezler from Marc Analysis as well as Rong-Chung Tyan and James Thomas at UCSD. This work is supported by Air Force Rome Laboratory.

9. REFERENCES

1. G.H. Haertling and C.E. Land, 'Hot-Pressed (Pb,La)(Zr,Ti)O_3 Ferroelectric Ceramics for Electrooptic Applications', J. Am. Ceram. Soc., Vol. 54, No. 1, pp. 1-10, 1971.

2. R. Viennet, ‘Driving Voltage Calculation for a Ferroelectric Display Device’, J. de Math. et de Phys. Appliquées, Vol. 29, pp. 715-22, 1978.

3. E.E. Klotin’sh, et al., ‘Geometrical Optics of an Electrically Controlled Phase Plate made of PLZT-10 Ferroelectric Ceramic’, Avtometriya, No. 6, pp. 68-72, 1984.

4. K. Tanaka, et al., ‘Analyses of PLZT Electrooptic Shutter and Shutter Array’, Jap. J. Appl. Phys., Vol. 24, No. 2, pp. 177-82, February 1985.

5. M. Title and S.H. Lee, ‘Modeling and characterization of embedded electrode performance in transverse electrooptic modulators’, Appl. Opt., Vol. 29, No. 1, pp. 85-98, January 1990.

6. Q. Wang Song, P.J. Talbot and J.H. Maurice, ‘PLZT based high-efficiency electro-optic grating for optical switching’, J. Modern Optics, Vol. 41, No. 4, pp. 717-27, 1994.

7. B. Mansoorian, *Design and Characterization of Flip-Chip Bonded Si/PLZT Smart Pixels (Ph.D. Thesis)*, Ch. 2, University of California, San Diego, 1994.

8. J. Thomas and Y. Fainman, ‘Programmable diffractive optical elements using a multichannel lanthanum-modified lead zirconate titanate phase modulator’, Opt. Lett., Vol. 20, No. 13, pp. 1510-12, July 1995.

9. A. Yariv and P. Yeh, *Optical Waves in Crystals*, Ch. 5, John Wiley and Sons, New York, 1984.

10. M. Ivey, ‘Birefringent Light Scattering in PLZT Ceramics’, *IEEE Transactions on Ultrasonics, Ferroelectrics, and Frequency Control*, Vol. 38, No. 6, pp. 579-84, IEEE, New York, 1991.

11. H. Elgan, ‘Excitation of Elastic Surface Waves by Spatial Harmonics of Interdigital Transducers’, *IEEE Transactions on Electron Devices*, Vol. 16, No. 16, pp. 1014-17, IEEE, New York, 1969.

12. A. Y. Wu, T. C. Chen and H.Y. Chen, ‘Model of electrooptic effects by green’s function and summary representation: applications to bulk and thin film PLZT displays and spatial light modulators’, *Proceedings of Eighth IEEE International Symposium on Applications of Ferroelectrics*, Eds. M. Liu, A. Safari, A. Kingon and G. Haertling, pp. 600-3, IEEE, New York, 1992.

13. G. Haertling, ‘Electro-optic ceramics and devices’, *Electronic Ceramics*, Ed. L. Levinson, pp. 371-492, M. Dekker, New York, 1988.